Vortex Modeling of Gaseous Jets in a Compressible Crossflow

S. D. Heister* and A. R. Karagozian†
University of California, Los Angeles, Los Angeles, California

This paper discusses an analytical/numerical model developed to describe the behavior of gaseous jets injected transversely into a subsonic (but compressible) crossflow. The cross section of the jet is modeled as an inviscid, compressible vortex pair, consistent with experimental observations of the transverse jet cross section. The numerically computed behavior of the vortex pair is used as an input to mass and momentum balances along the jet, forming a model that describes the trajectory, entrainment, and mixing of jets injected into subsonic crossflows in the range $0.15 \leq M_\infty \leq 0.8$. Theoretical predictions of jet trajectories are compared with limited experimental data, yielding accuracy within 10%. Because very short computational times are required for this model, it could serve as an excellent design tool for perfectly expanded or slightly underexpanded jets in subsonic crossflow.

Nomenclature

B = constant used in defining jet cross-sectional area
d = jet orifice diameter
F_y = dimensionless force tending to separate vortices due to compressibility associated with vortex pair
F_{yp} = dimensionless force tending to separate vortices due to jet underexpansion
h = dimensionless vortex pair half-spacing
I = dimensionless jet impulse per unit depth at the orifice
k = recirculation cell perimeter-to-area ratio
M = Mach number
p = dimensionless pressure
R = jet-to-crossflow momentum ratio $\equiv p_{jo}U_{jo}^2$
s = dimensionless distance measured along jet trajectory
t = dimensionless time
U = dimensionless velocity
w = dimensionless mass-per-unit depth within jet cross section
x_0 = dimensionless x-intercept of stagnation streamline
X = streamwise coordinate of jet trajectory
y_0 = dimensionless y-intercept of stagnation streamline
Z = transverse coordinate of jet trajectory
γ = ratio of specific heats
Γ = dimensionless vortex strength
ρ = dimensionless density
ϕ_v = jet orientation angle

Subscripts

c = recirculation cell condition
j = jet conditions
jo = jet conditions at orifice
∞ = freestream conditions

Superscript

$(^-)$ = dimensional quantity

Presented as Paper 88-3720 at the AIAA/ASME/SAE/ASEE 24th Joint Propulsion Conference, Boston, MA, July 11-13, 1988; received July 18, 1988; revision received Dec. 7, 1988.

*Graduate Research Assistant, Mechanical, Aerospace and Nuclear Engineering Department; currently Section Head, The Aerospace Corporation.

†Associate Professor, Mechanical, Aerospace and Nuclear Engineering Department. Member AIAA.

Introduction

THE transverse jet is a classical problem in fluid mechanics that has several applications of practical importance including fuel jets injected in turbojet, ramjet, and scramjet combustors, dilution jets for local cooling in turbojet engines or external components of aerospace vehicles, thrust vector control systems, and vertical or short takeoff and landing aircraft. The goal of the modeling described in this paper is to describe the trajectories and downstream mixing of single gaseous jets injected transversely through a circular orifice into a uniform compressible (subsonic) stream of fluid. It is of particular interest to be able to develop a model that can be used as a design tool, i.e., one that requires a minimum of computational time.

Although there has been much research into the behavior of transverse jets in low-speed (incompressible) and supersonic crossflows, surprisingly little has been published regarding flow in the subsonic (but compressible) regime. Early supersonic flow experiments were conducted by Spaid and Zukoski.[1-3] These researchers likened the jet to a hemispherical body, and by developing a force balance on this imaginary body, they were able to correlate jet penetration with injection and crossflow parameters. Similar models have been developed by Hsia[4] for the case of a supersonic crossflow and Manela and Seginer[5] for the case of a transonic crossflow. The model of Manela and Seginer appears as one of the few models applicable to the high subsonic range, but suffers from the fact that the actual jet trajectory and mixing are not calculated. Experimental studies by Manela and Seginer do provide data on jet trajectories, however.

As early as 1963, Abramovich[6] described the cross section of a transverse jet as elliptical or "kidney shaped" due to the pressure/shear field imposed by the freestream flow. In the 1970's, experiments by Fearn and Weston[7] and Kamotani and Greber[8] revealed a vortex pair structure associated with jets in low-speed crossflows. Fearn and Weston[7] and LeGrives[9] made use of these observations to develop semiempirical vortex models for computing trajectories of gaseous jets in incompressible crossflows.

More recently, Karagozian and co-workers[10-13] developed analytical models for nonreacting and reacting jets in crossflow that represent the jet cross section as a pair of counter-rotating vortices in an incompressible uniform stream. The models are locally two-dimensional and assume the jet (or, with a reaction, the "flame") cross section to be comprised of a counter-rotating, viscous vortex pair separated by a distance $2\tilde{h}$. Upon introduction of the uniform crossflow locally perpendicular to the jet, the resulting cross section is approxi-

mately that of the classical Kelvin oval. Viscous effects act to separate the vortices downstream. The model also incorporates a momentum balance along the jet as well as a representation for vortex strength, which accounts for jet impulse and viscous forces at the periphery of the jet orifice. Ultimately, jet trajectories, cross-sectional area, flame lengths, and other characteristics are predicted and compared favorably with experimental results.

This type of vortex model cannot be used in the case of a highly compressible subsonic or supersonic jet or cross stream, but the general approach does eliminate several of the deficiencies associated with previous transverse jet models. The major difficulty in applying the technique lies in representation of a compressible vortex pair. The very recent work of Moore and Pullin[14] and Heister et al.[15,16] suggests that a solution for the flow about a compressible vortex pair is possible, which can serve as a basis for a compressible version of the Karagozian model. In particular, the numerical solution in Heister[16] provides the shape of the vortex pair recirculation cell and the force that tends to separate the compressible vortices, which, in conjunction with one-dimensional mass and momentum balances along the jet, permits calculation of the jet trajectory. This paper presents a description of this subsonic crossflow model and a parametric summary of results and comparison with limited experimental data.

Vortex Modeling and the Compressible Vortex Pair Solution

Figure 1 provides a schematic description of a gas jet in a subsonic crossflow. The boundary layer along the wall is neglected here, since this is a low-momentum region in which little jet turning occurs. One-dimensional isentropic flow is assumed to take place along the jet, so that shock structures associated with highly underexpanded jets will not be considered. However, if the jet is only slightly underexpanded, then shocks within the jet are weak, and the isentropic assumption is approximately valid.

The jet cross section is assumed to be comprised of a pair of counter-rotating, compressible vortices with dimensionless circulations $\pm\Gamma$, separated by a dimensionless distance $2h$. Vortex strength is nondimensionalized by freestream velocity and the jet orifice diameter, whereas vortex half-spacing is nondimensionalized by orifice diameter. The local velocity perpendicular to the cross section is related to the sine of the jet orientation angle ϕ_v. Solution of the flowfield associated with the compressible vortex pair allows calculation of a net force tending to separate the vortices F_y, which is a function of $M_\infty \sin\phi_v$. This force results from compressibility effects only. If the jet is underexpanded, an additional force F_{yp} tends to drive the vortices apart.

All jet and freestream conditions are nondimensionalized using freestream density ρ_∞ and velocity U_∞, as well as the orifice diameter d. There are six basic dimensionless parameters that completely describe the jet injection process. These parameters include the jet and freestream Mach numbers (M_j, M_∞), the jet and freestream ratio of specific heats (γ_j,γ), the jet-to-crossflow velocity ratio (U_{jo}), and the jet-to-crossflow momentum flux ratio R, which is defined as

$$R \equiv \rho_{jo} U_{jo}^2 \tag{1}$$

Here, ρ refers to gas density, and jo refers to the conditions at jet injection, each nondimensionalized by freestream conditions. We note in passing that our definition of R is the square of the definition employed by other researchers[7,10]; it may also be expressed in terms of the initial jet-to-crossflow pressure ratio p_{jo}/p_∞,

$$R = \gamma_j p_{jo} M_j^2 / (\gamma p_\infty M_\infty^2) \tag{2}$$

where pressures are rendered nondimensional using freestream density and velocity. Clearly, ρ_{jo}, p_{jo}, and p_∞ are not initial inputs, but may be calculated in terms of input quantities:

$$\rho_{jo} = R/U_{jo}^2 \tag{3}$$

$$p_{jo} = R/(\gamma_j M_j^2), \qquad p_\infty = 1/(\gamma M_\infty^2) \tag{4}$$

and in the nondimensionalization employed, $\rho_\infty = U_\infty = 1$.

In order to calculate the force acting to separate the vortices, the complete solution for the flowfield associated with a compressible vortex pair in crossflow is required. Figure 2 highlights some of the physical differences between compressible and incompressible vortex pair recirculation cells. The incompressible cell enjoys a symmetry about both x and y axes, with dimensionless intercepts at $x_0 = \pm\sqrt{3}h$, $y_0 \simeq \pm 2.09h$. The compressible cell is complicated by the presence of vacuum cores that surround each vortex center, and the possibility of

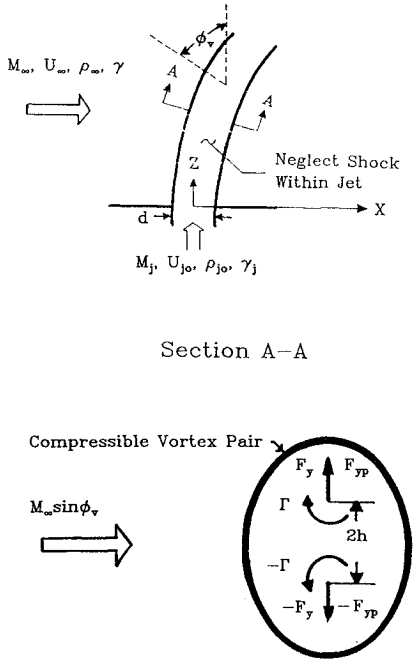

Fig. 1 Schematic description of a gaseous jet in a subsonic crossflow.

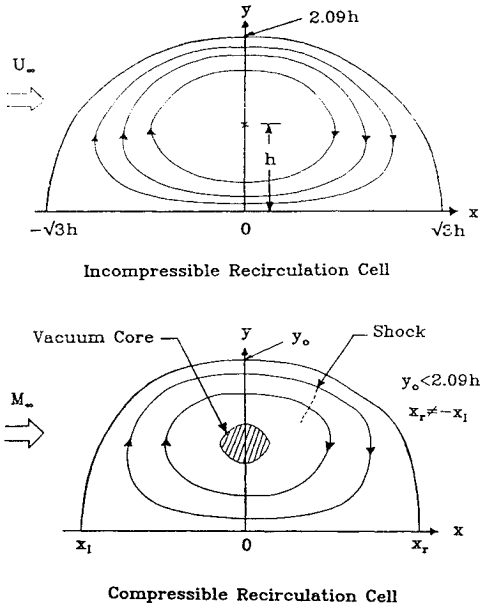

Fig. 2 Comparison of features of incompressible and compressible vortex pair recirculation cells.

a shock existing in the recirculating region for $x>0$. The vacuum cores arise from the fact that there is a maximum achievable flow speed in a compressible fluid at which vacuum conditions exist. Since for a compressible vortex one can show that $qr = \text{const}$, where q is the flow speed and r the radial distance from the vortex center, we must have a vacuum region surrounding the center of any compressible vortex. The vacuum increases in size as the freestream Mach number increases. Interested readers are referred to Heister[16] for further discussion of the numerical solution used as input to the present gas jet model.

Model for the Gaseous Jet in Subsonic Crossflow

Results from the computed flowfield associated with a compressible vortex pair are now utilized in the compressible transverse jet model. To reduce computational time and improve model efficiency, results are curve fit as a function of upstream Mach number. Problems associated with the numerical scheme prohibit accurate solutions beyond $M_\infty = 0.3$, so that extrapolation is required to encompass the larger Mach number range of the gas jet model. The vacuum core surrounding the vortices becomes a dominant factor above $M_\infty = 0.66$, so that a logical extension of the results for lower M_∞ must be applied for crossflow Mach numbers exceeding this value. The results of the curve fits are presented below:

$$\rho_c = 1.0 - 0.76(M_\infty \sin\phi_v) \tag{5a}$$

$$k = [1.024 + 1.4(M_\infty \sin\phi_v)^2]/h \tag{5b}$$

$$F_y = [3.02(M_\infty \sin\phi_v)^{0.7}]hp_j/p_c \tag{5c}$$

where ρ_c is the average dimensionless recirculation cell density, k represents the ratio of cell perimeter to cell area, and F_y represents the dimensionless net force tending to separate the vortices. The pressure ratio in the F_y expression is required in order to scale forces up or down with respect to the current jet pressure p_j. The cell pressure p_c is calculated using the constant entropy assumption

$$p_c = \rho_c^{\gamma_j}/(\gamma_j M_\infty^2 \sin^2\phi_v) \tag{6}$$

and the jet pressure is calculated from jet density in a similar manner.

The quantity F_y is obtained by integrating the net pressure force on a closed streamline obtained from the compressible vortex pair solution. This force arises due to the fact that a vacuum core surrounds each vortex center and that shocks may be present in the recirculating region. Equations (5) shows that F_y vanishes as $M_\infty \to 0$, which is consistent with the incompressible vortex pair solution in that this flowfield contains no vacuum core and has no net force separating the vortices. In this limit, viscous forces tend to dominate the vortex pair separation process, as indicated by Karagozian.[10] Although viscous effects are difficult to study in the case of the compressible vortex pair, order of magnitude estimates indicate that in the compressible flow regime under consideration, viscous effects are not as important to vortex separation as are compressibility effects.

Pressure Force for Underexpanded Jets

If the jet is underexpanded, an additional force tends to separate the vortices. Figure 3 describes schematically the case where a one-dimensional situation ($p_j = \text{const}$, $p_\infty = \text{const}$) is assumed as a first approximation. The net pressure imbalance occurs at the jet periphery where we can write

$$F_p = \int_0^\ell (p_j - p_\infty)\, d\ell \cdot \hat{j} = x_0(p_j - p_\infty) \tag{7}$$

where $\hat{j}$ is a unit vector in the y direction. Now if we assume a uniform dilatation of the line segment connecting the vortex center and the vector boundary, the net force experienced at the vortex center becomes

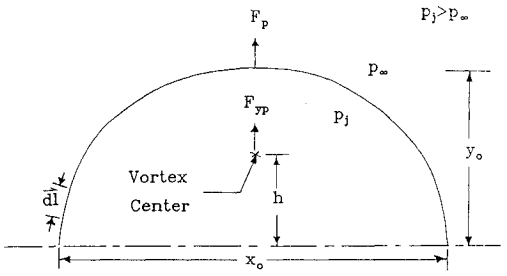

Fig. 3 Schematic description of pressure force F_{yp} for an underexpanded jet.

$$F_{yp} = (x_0/y_0)(p_j - p_\infty)h \tag{8}$$

Results of Heister's[16] compressible vortex pair solutions indicate that recirculation cell size is such that $x_0/y_0 \approx 1.66$ for the entire Mach number range under consideration. Although this treatment is only approximate, recall that we are only considering slightly underexpanded jets, so that a pressure equilibrium is reached within 2-3 jet diameters of the orifice. For this reason, this approximate treatment for F_{yp} is appropriate.

Local Jet Orientation Angle ϕ_v

Following Karagozian,[10] we can develop a relation for the local jet orientation angle ϕ_v defined in Fig. 1. The relation is really one for vortex circulation due to jet impulse and viscous forces acting at the jet periphery. If bars denote dimensional quantities, we may write

$$\bar{\Gamma} = 2\bar{U}_\infty \bar{d} \sin\phi_v + [\bar{I}/(2\bar{\rho}_\infty \bar{h})] \cos\phi_v \tag{9}$$

where $\bar{I}$ is the initial impulse per unit length along the jet. For the underexpanded jet, $\bar{I}$ takes the form

$$\bar{I} = (\bar{\rho}_{jo}\bar{U}_{jo}^2 + \bar{p}_{jo} - \bar{p}_\infty)\pi\bar{d}^2/(4\bar{U}_\infty) \tag{10}$$

The coefficient of $\sin\phi_v$ in Eq. (9) describes the component of circulation arising from viscous forces as the crossflow is deflected about the jet orifice, while the coefficient of $\cos\phi_v$ represents circulation generated in the flowfield by the jet's impulse. The model for vorticity generation indicated in Eq. (9) has been shown to adequately represent the local vortex strength exposed when slices of the jet are taken at the local angle ϕ_v. For a more complete description of these forces, see Karagozian[10] or Broadwell and Breidenthal.[17] The nondimensional form of Eq. (9) can be written strictly in terms of h, ϕ_v, and known input variables

$$\Gamma = 2 \sin\phi_v + \frac{\pi}{8h}[R + R/(\gamma_j M_j^2) - 1/(\gamma M_\infty^2)] \cos\phi_v \tag{11}$$

The circulation in Eq. (11) must be exactly balanced by the local circulation of the vortex pair Γ_v, derived from the upwash velocity of the pair in crossflow

$$\Gamma_v = 4\pi \sin\phi_v F(M_\infty) \tag{12}$$

where $F(M_\infty)$ is a compressibility correction factor. Moore and Pullin[14] describe this correction factor for small M_∞ as

$$F(M_\infty) = (1 - M_\infty^2/4)^{-1} \tag{13}$$

which tends to increase the dimensionless circulation above the incompressible value of 4π. The correction is less than 10% at $M_\infty = 0.5$, and since the actual form of $F(M_\infty)$ is not known

for higher M_∞, we assume here that $F(M_\infty) \cong 1$. Incorporating this assumption and equating Eqs. (11) and (12) gives the governing relation for ϕ_v in terms of h:

$$\sin\phi_v = \left\{ \left[\frac{(4\pi h - 2)8h/\pi}{R + R/(\gamma_j M_j^2) - 1/(\gamma M_\infty^2)} \right]^2 + 1 \right\}^{-1/2} \tag{14}$$

Initially, we require a transverse injection ($\sin\phi_v = 1$), so that the initial condition for h becomes

$$h_0 = (2\pi)^{-1} \tag{15}$$

Force Balance in Jet Cross Section

Referring to Fig. 3, we can apply Newton's second law to the upper vortex:

$$\frac{\mathrm{d}}{\mathrm{d}t}\left(w_j \frac{\mathrm{d}h}{\mathrm{d}t}\right) = F_y + F_{yp} \tag{16}$$

where w_j is the dimensionless mass-per-unit length within the upper half of the recirculation cell, which changes with "flow" time t, measured along the jet trajectory. The mass can be written

$$w_j = \rho_j B h^2 \tag{17}$$

where Bh^2 represents the area of the upper half of the recirculation cell. The constant B can be determined by setting the initial recirculation cell area equal to the orifice area:

$$B = \pi^3/2 \tag{18}$$

Now w_j is dependent on flow time since the mass balance along the jet incorporates the effects of entraining the outer flow. Therefore, performing the evaluation of Eq. (16) yields

$$\frac{\mathrm{d}^2h}{\mathrm{d}t^2} = \frac{F_y + F_{yp}}{w_j} - \left(\frac{1}{\rho_j}\frac{\mathrm{d}\rho_j}{\mathrm{d}t} + \frac{2}{h}\frac{\mathrm{d}h}{\mathrm{d}t}\right)\frac{\mathrm{d}h}{\mathrm{d}t} \tag{19}$$

a second-order ordinary differential equation in h. Relation (15) provides the initial value of h required for integration of Eq. (19), but a second initial condition is required. We follow the procedure of Karagozian[10] and assume a power law behavior near $t = t_0$, the initial flow time

$$h = at^\alpha, \qquad \rho_j = bt^\beta \tag{20}$$

Note that ϕ_v is an additional time-dependent function, but $\sin\phi_v$ varies slowly initially, so we can approximate $\sin\phi_v \cong 1$ in order to calculate the initial F_y value. Substituting Eq. (20) into Eq. (19) and using Eqs. (5) and (18) gives a relation involving a, b, α, β, and t. We note that

$$p_j \propto \rho_j^{\gamma_j} t^{\beta\gamma_j}$$

so that the pressure variation is simply a function of β. Equating exponents in the relation yields the following result:

$$\alpha = 1, \qquad \beta = 0 \tag{21}$$

This contrasts the $h \propto t^{1/2}$ behavior observed by Karagozian[10] in the case of the incompressible gas jet. Using Eq. (21) and the value of h_0, we can then solve the governing relation for t_0, the initial flow time

$$t_0 = [w_{jo}h_0/(F_{yo} + F_{ypo})]^{1/2} \tag{22}$$

where o refers to the "initial" state, where $\phi_v = 90$ deg. Given the initial flow time, we can determine the initial slope

$$\left(\frac{\mathrm{d}h}{\mathrm{d}t}\right)_{t=t_0} = h_0/t_0 \tag{23}$$

and all initial conditions for the differential equation are prescribed.

Mass and Momentum Balances Along the Jet

The final elements required to complete the gas jet model are relations for the average jet density and velocity as a function of flow time. As mentioned previously, entrainment of the outer flow is considered and will tend to decelerate or accelerate the jet, depending on the local jet orientation. For underexpanded jets, entrainment is not considered until $p_j = p_\infty$, since we have no way of estimating contributions of jet expansion and entrainment with a single mass balance equation. Therefore, in this case the jet mass flow must be constant, and the jet density is simply calculated using

$$\frac{\mathrm{d}\rho_j}{\mathrm{d}t} = -2\left(\frac{\rho_j}{h}\right)\frac{\mathrm{d}h}{\mathrm{d}t}, \qquad (p_j > p_\infty) \tag{24}$$

which requires that all of the area change in the recirculation cell corresponds to a change in cell density. Once the jet has expanded to the local pressure, entrainment of additional fluid is permitted and we may write

$$\frac{\mathrm{d}\rho_j}{\mathrm{d}t} = -\frac{2\rho_j}{h}\frac{\mathrm{d}h}{\mathrm{d}t} + k\cos\phi_v, \qquad (p_j = p_\infty) \tag{25}$$

where k is given in Eqs. (5). The entrainment represented in the second term on the right side of Eq. (25) has been calculated assuming mass addition around the entire jet periphery at a mass flux of $\rho_\infty U_\infty \cos\phi_v$, which represents the local free-stream flux parallel to the jet axis.

A momentum balance along the jet will provide as a relation for the average jet axial velocity U_j. We consider momentum changes due to mass addition and possible pressure changes:

$$\dot{m}\frac{\mathrm{d}U_j}{\mathrm{d}t} = \frac{\mathrm{d}\dot{m}}{\mathrm{d}t}(U_e - U_j) - Bh^2\frac{\mathrm{d}p_j}{\mathrm{d}t} \tag{26}$$

where $\dot{m} = w_j U_j$ is the jet mass flow rate, and U_e is the velocity of the entrained fluid, assumed to be equal to $U_\infty \cos\phi_v$. The pressure derivative can be expressed in terms of density using $p_j\rho_j^{\gamma_j}$ = constant, so that Eq. (26) can be rewritten:

$$\frac{\mathrm{d}U_j}{\mathrm{d}t} = \left[\frac{1}{\rho_j}\frac{\mathrm{d}\rho_j}{\mathrm{d}t}\left(\cos\phi_v - U_j - \frac{\gamma_j p_j}{\rho_j U_j}\right) + \left(\cos\phi_v - U_j\right)\frac{2}{h}\frac{\mathrm{d}h}{\mathrm{d}t}\right] \div \left(2 - \frac{\cos\phi_v}{U_j}\right) \tag{27}$$

yielding a relation in terms of ρ_j and h derivatives alone. Given the U_j resulting from solution of Eq. (26), the dimensionless jet coordinates (X,Z), shown in Fig. 1, can be obtained using a simple integration:

$$X = \int_{t_0}^{t} U_j \cos\phi_v \, \mathrm{d}t \tag{28a}$$

$$Z = \int_{t_0}^{t} U_j \sin\phi_v \, \mathrm{d}t \tag{28b}$$

This completes the description of the model.

Equations (19), (25), and (27) are integrated numerically using Huen's method. Huen's method is a second-order trapezoidal scheme presented in most texts on numerical analysis.[18] A nondimensional step size of 0.05 is used for all cases. Inte-

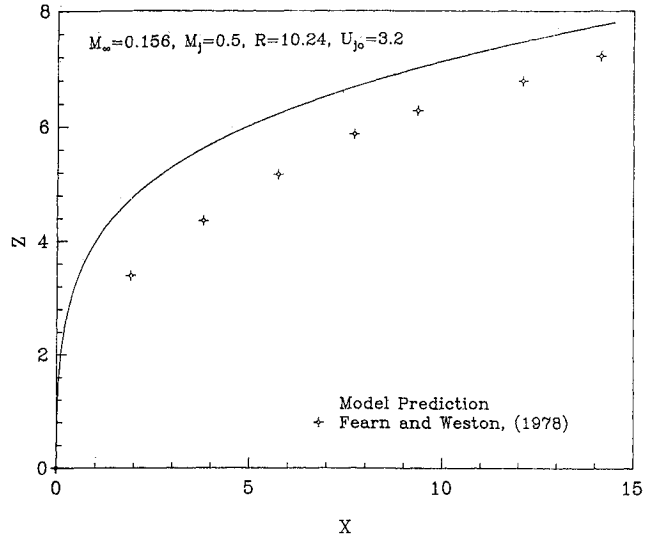

Fig. 4 Comparison of theoretical and experimental results for jet trajectory at $M_\infty = 0.156$.

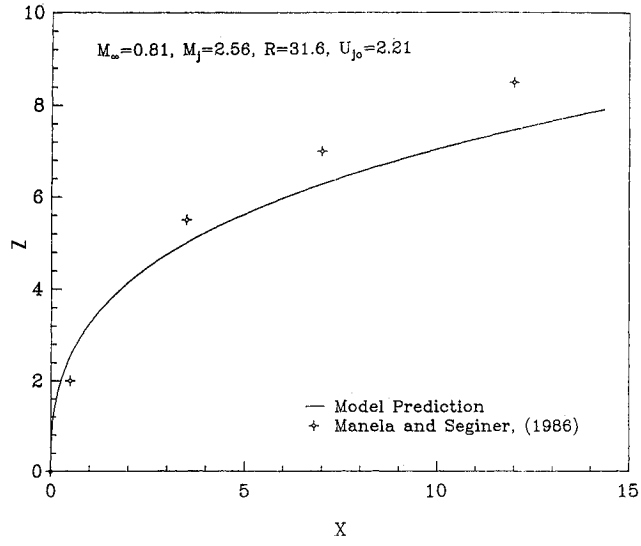

Fig. 6 Comparison of theoretical and experimental results for jet trajectory at $M_\infty = 0.81$.

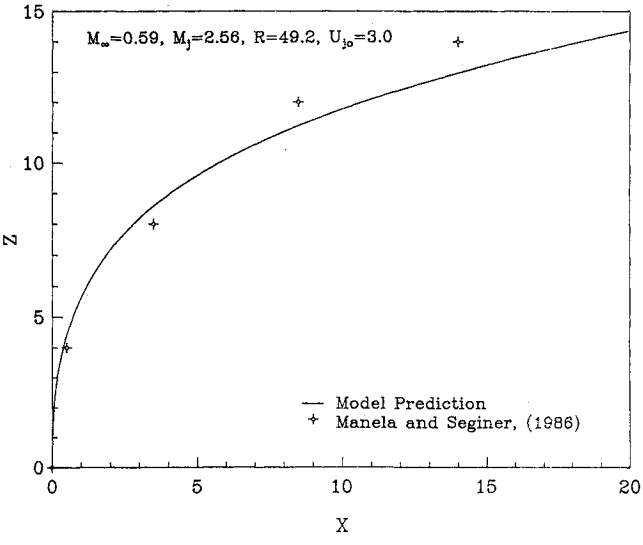

Fig. 5 Comparison of theoretical and experimental results for jet trajectory at $M_\infty = 0.59$.

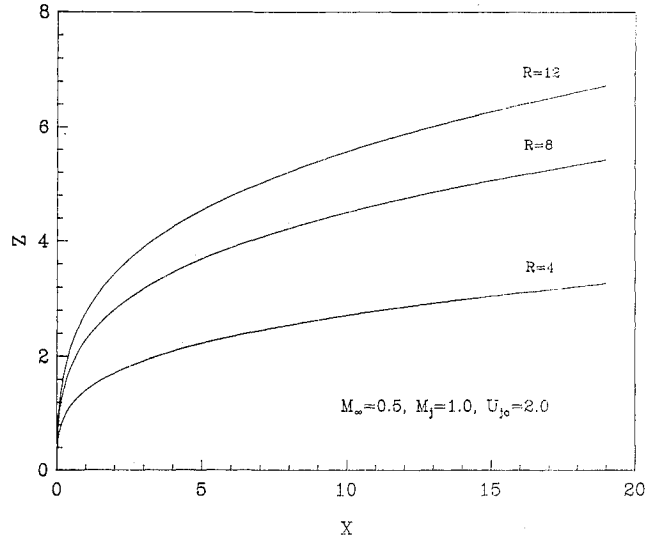

Fig. 7 Effect of increasing momentum ratio R on jet trajectory.

gration in Eqs. (28) is performed using a second-order trapezoidal method.

The resulting computer code generated using the numerical technique described previously represents a simple closed-form description of the transverse jet. The code is only about 200 lines and runs in only a few seconds on the IBM 3090 computer. Typical runs contain 400-600 points along the jet trajectory. The simplicity of the code enables many comparisons and parametric studies to be made using a minimal amount of computer time.

Results

In this section, we first compare vortex model calculations with experiments and then investigate the effects of varying each of the input parameters governing the jet injection. Unfortunately, very little experimental data exist in the range $0.15 < M_\infty < 0.66$, which is the range in which the current compressible vortex pair solution is valid. However, the recent paper by Manela and Seginer[5] does provide some jet trajectory data in this range. In addition, comparisons can be made with a low Mach number experiment conducted by Fearn and Weston.[7]

Although most of Fearn and Weston's data are for the incompressible regime, one run was made at $M_\infty = 0.156$, barely within the range of applicability of the model. A comparison of the experimental and analytical results for the jet trajectory is provided in Fig. 4. The model tends to overpredict jet penetration, but does follow the shape of the trajectory well for much of the curve. The overshoot is due to the fact that no viscous force tending to separate the vortices has been included in the model. The viscous, incompressible model of Karagozian[10] is more valid in this lower Reynolds number flow regime and actually predicts the trajectory more closely.

Figure 5 shows good comparison at $M_\infty = 0.59$ with the experimental data of Manela and Seginer.[5] The jet is slightly underexpanded ($p_j/p_\infty = 2.6$) and verifies the significance of the pressure imbalance force F_{yp} incorporated in the model. Extrapolation of compressible vortex pair results to $M_\infty = 0.81$ permits a comparison with experimental data of Manela and Seginer at this Mach number, as shown in Fig. 6. In this case, overall jet penetration is underestimated by about 10%, but

reasonable agreement is present over the entire trajectory. Thus, the extrapolation appears to give reasonable results despite a diminished accuracy in the compressible vortex pair solution.

As discussed in the section on vortex modeling, when we nondimensionalize using ρ_∞, U_∞, and d, the six independent parameters describing the jet injection problem are M_∞, M_j, γ, $\gamma_j U_{jo}$, and R. Values of the freestream ratio of specific heats γ are assumed to be 1.4 throughout, whereas a series of runs are conducted to assess the importance of the other five variables. Trajectories for γ_j variations between 1.2 and 1.4 are essentially identical, which implies that this parameter is of secondary importance to description of the resultant jet trajectory. This result agrees with the conclusions of Chrans and Collins,[19] who find no influence of jet characteristics due to injectant molecular weight. Thus, by eliminating γ and γ_j from our list of parameters, we investigate the effects of the remaining four variables.

Figure 7 demonstrates the importance of the momentum flux ratio R in determining jet trajectories. The three R values shown correspond to injection pressure ratios between 1 (for the $R = 4$ case) and 3 (for the $R = 12$ case). Since U_{jo} is fixed for all three cases, increasing R corresponds to increasing the density ratio, and the threefold increase between upper and lower curves yields a 100% increase in overall jet penetration.

In Fig. 8, we note the relative insensitivity of jet penetration to the initial velocity ratio U_{jo}. For the fixed R value of 16, increasing U_{jo} tends to decrease overall penetration slightly. In other words, for a fixed jet momentum, the low-density, high-velocity jet realizes a slightly better penetration. This is due to the fact that the high-speed jets realize a slightly better initial penetration into the crossflow. The effect, however, is minor, since a doubling of U_{jo} decreases overall penetration by only 12%.

Returning to the parameters selected for Fig. 7, Fig. 9 presents vortex half-spacing h as a function of time. The gradients in h tend to increase as the jet becomes more underexpanded (increasing R) due to the F_{yp} force discussed previously. Although the behavior near the orifice is linear, the overall character is similar to that of the incompressible formulation of Karagozian.[10,11]

The rapid increase in half-spacing h near $t = t_0$ (the jet orifice condition) generates a large degree of entrainment of the outer flow, as evidenced in Fig. 10. In this figure, the fluid entrainment ratio E and distance s are defined

$$E = \rho_j U_j h^2/(\rho_j U_{jo} h_0^2) \tag{29a}$$

$$s = \int_{t_0}^{t} U_j \, dt \tag{29b}$$

The curves in Fig. 10 indicate that mixing of the jet and outer flow decreases with increasing jet momentum. The one-dimensional analysis along the jet probably leads to an underprediction of effective mixing length, although we are aware of no data with which to verify this conclusion. A more refined model may treat the jet axisymmetric density and velocity distributions and should provide better mixing length and entrainment predictions.

The effects of jet underexpansion on jet velocity are illustrated in Fig. 11 where $R = 4$ corresponds to a perfectly expanded jet, and $R = 12$ corresponds to $p_j/p_\infty = 3$. The underexpanded jet experiences a rapid velocity increase associated with the expansion to freestream conditions and reaches a maximum value of 2.47 just 0.22 jet diameters from the orifice. Thus, underexpansion effects are confined to a relatively small region, as discussed earlier. It is also interesting to note that in both cases, the jet velocity actually drops below the freestream velocity and asymptotically approaches $U_j = U_\infty = 1$ as $\phi_v \to 0$ deg.

Figure 12a illustrates the drastic effect that increasing the freestream Mach number M_∞ has on a perfectly expanded,

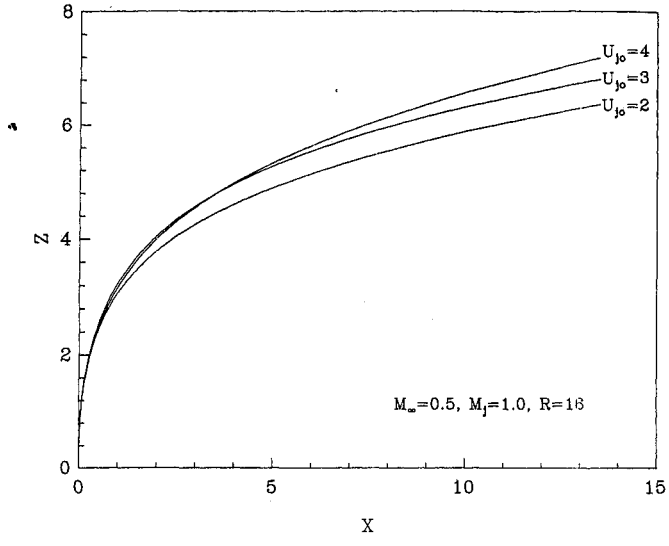

Fig. 8 Effect of jet-to-crossflow velocity ratio U_{jo} on jet penetration.

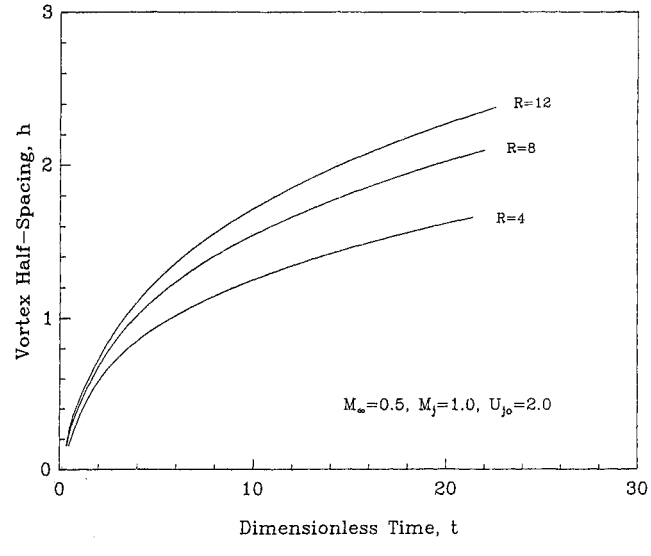

Fig. 9 Vortex half-spacing histories.

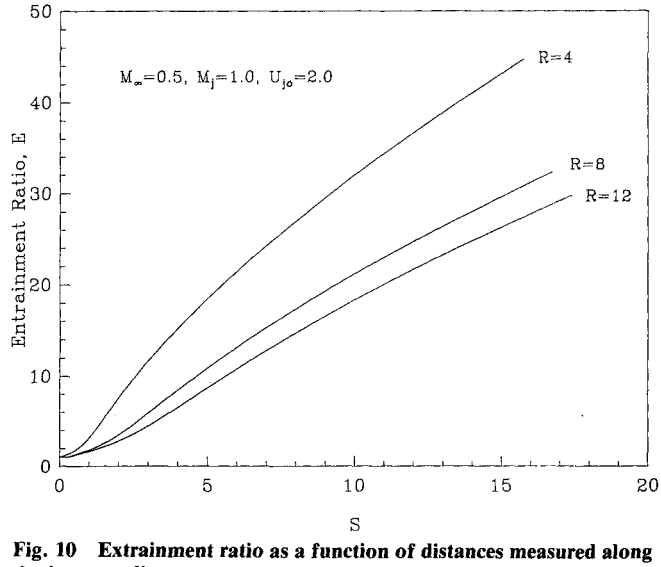

Fig. 10 Extrainment ratio as a function of distances measured along the jet centerline.

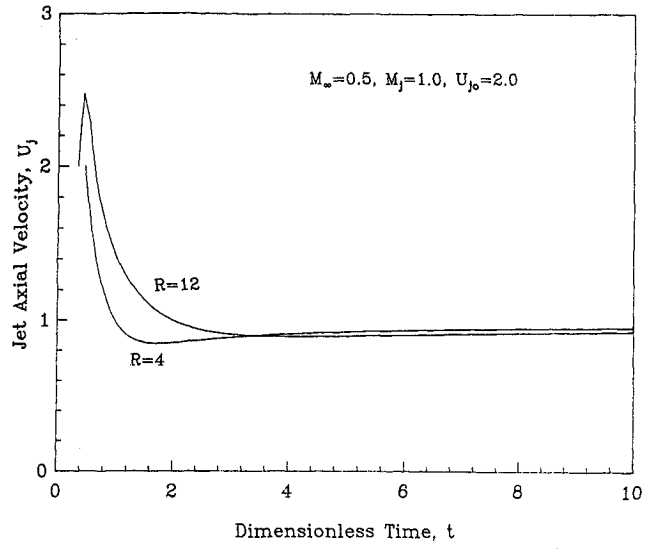

Fig. 11 Jet axial velocity histories for perfectly expanded (R = 4) and underexpanded (R = 12) jets.

constant-density jet. In increasing M_∞ from 0.25 to 0.75, overall penetration is reduced by 84%, which is not surprising since R drops by a factor of 9 with this increase in M_∞. Figure 12b demonstrates that M_∞ is still an important parameter even when jet-to-crossflow momentum ratio is held fixed. The primary factor causing this result is the increased vortex pair separation force F_y at higher M_∞ values. Inclusion of shock losses within the jet would make the comparison even more dramatic than Fig. 12b since the M_∞ = 0.75 jet is highly underexpanded (p_{jo}/p_∞ = 9).

The final parameter to investigate is the jet injection Mach number M_j, which is varied from 1 to 3 in Fig. 13. In this figure, jet reservoir stagnation conditions are held fixed (p_{0j} = 105, ρ_{0j} = 13.1) so that the effects of various nozzle expansion ratios can be determined. Nozzle expansion ratios of 1, 1.69, and 4.23 correspond to M_j = 1, 2, and 3, respectively. The momentum ratios corresponding to M_j = 1, 2, and 3 are R = 78, 75, and 36, which demonstrates the large effects on dynamic pressure when expanding a compressible fluid. The higher velocity associated with M_j = 2 jet tends to overcome the lower density, giving a slightly better penetration than the sonic jet. This difference shown is not that significant, although the sonic jet is highly underexpanded (p_j/p_∞ = 19), so that shock losses in this jet will tend to reduce its penetration

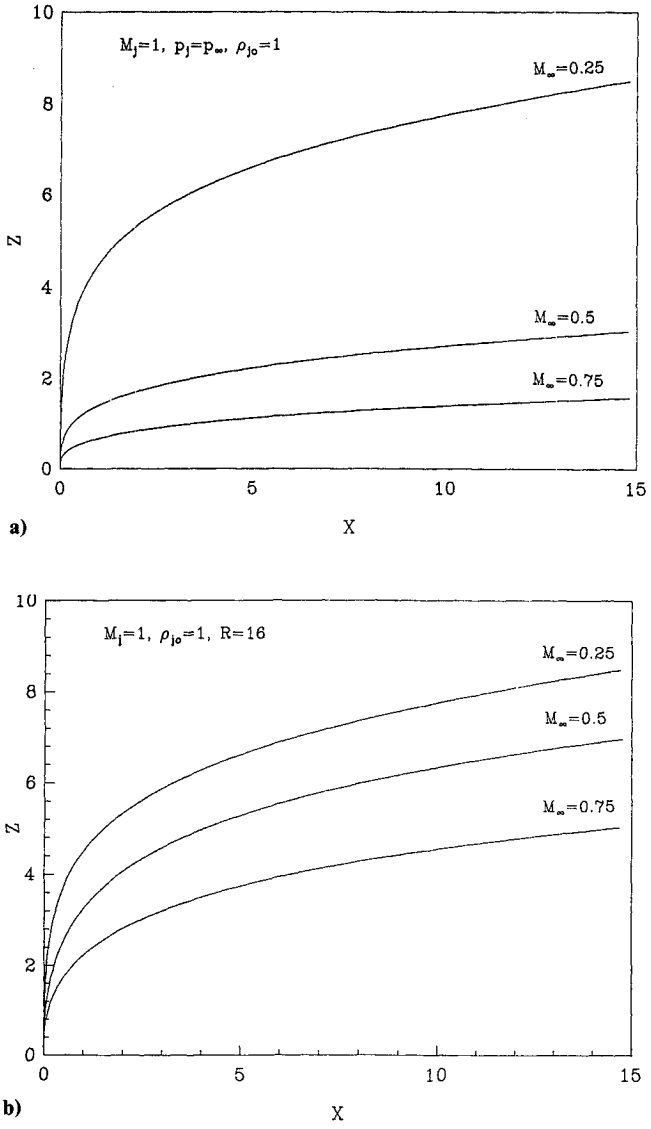

Fig. 12 Effects of increasing freestream Mach number a) for a perfectly expanded, constant-density jet where R is varied; b) for conditions where R = 16 is held fixed.

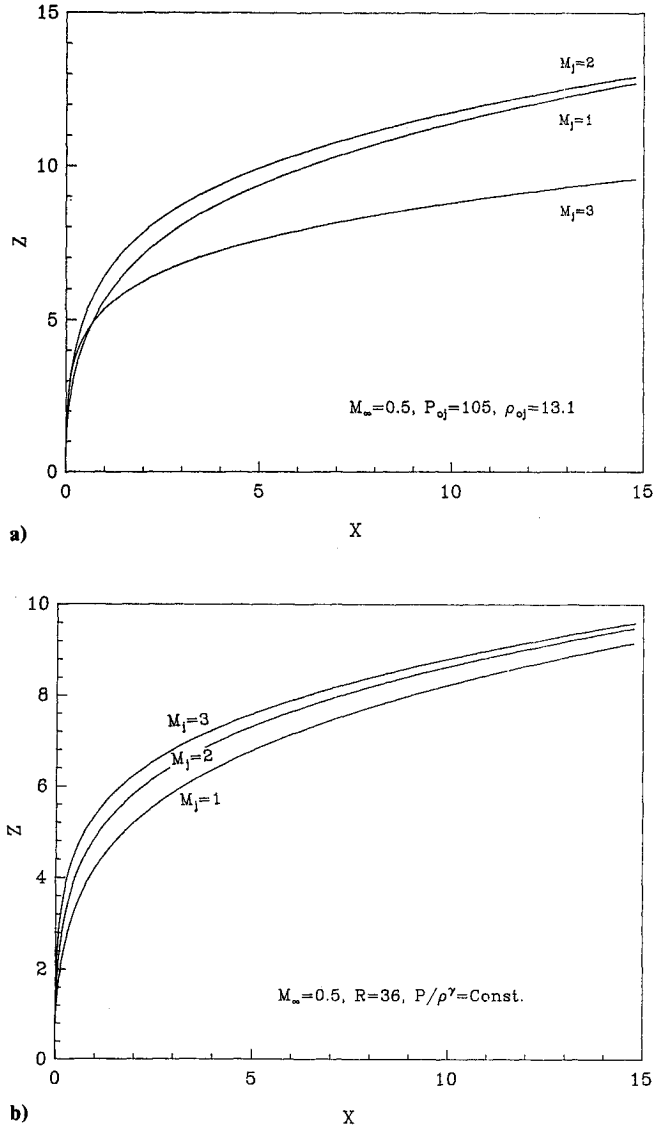

Fig. 13 Effects of injection Mach number on jet trajectory a) for given jet stagnation conditions; b) for conditions where R = 36 is held fixed.

from that shown in Fig. 13. For this reason, we see that a slightly supersonic injection is desirable to enhance penetration of a compressible transverse jet. Of course, R losses associated with very high M_j injection preclude this case from consideration. When R is held fixed and M_j is varied, as shown in Fig. 13b, we observe that very little change in penetration occurs. Since shock losses within the jet are not considered, keeping constant jet momentum implies a nearly constant penetration. If shock losses were included, the $M_j = 1$ jet would have reduced penetration, since it is highly underexpanded ($p_{j_0}/p_\infty = 9$).

Summary and Discussion

The vortex model presented in the present paper is useful in determining the extent of penetration of perfectly or slightly underexpanded gaseous jets in subsonic crossflow. Model limitations are such that accuracy is diminished at freestream Mach numbers below 0.15 and above 0.8, although reasonable results are obtained for flows slightly outside this range.

To consider highly underexpanded jets, a model for jet shock structure must be included to account for momentum losses within the jet. In the future, such a model could be created by following the ideas of Adamson and Nicholls,[20] who describe a technique to analyze an underexpanded jet issuing into quiescent fluid. However, from a practical standpoint, highly underexpanded jets are not desirable, since momentum losses in the Mach disk within the jet become prohibitive (see Schetz and Billig[21] for further discussion).

One-dimensional mass and momentum balances along the jet are adequate to predict jet trajectories, but probably do not predict mixing length or degree of entrainment as accurately. Future efforts will be aimed at correcting this shortcoming by refining mass and momentum balances along the jet.

The results shown in Figs. 7–13 indicate the importance of the injection parameters R, M_j, and M_∞ for prediction of the jet trajectory and penetration. For some transverse jet applications, it may be desirable to achieve a constant penetration over the entire M_∞ range encountered. To meet this requirement, a mechanism should be included to keep jet-to-crossflow momentum ratios fairly constant. One could use metering devices to lower the jet reservoir pressure at low M_∞ values and raise this pressure as M_∞ increased.

Figure 13a highlights the desirability of slightly supersonic injection to maximize jet penetration. Parametric analysis would be required to optimize nozzle design, but it appears that fairly small expansion ratios appear as optimum. A good injector nozzle design can minimize shock losses within the jet and enhance overall penetration.

Acknowledgment

The authors wish to acknowledge the support of NASA Ames/Dryden Research Center under Grant NCC-2-374.

References

[1]Zukoski, E. E. and Spaid, F. W., "Secondary Injection of Gases into a Supersonic Flow," *AIAA Journal,* Vol. 2, Oct. 1964, pp. 1689–1696.

[2]Spaid, F. W. and Zukoski, E. E., "Further Experiments Concerning Secondary Injection of Gases into a Supersonic Flow," *AIAA Journal,* Vol. 4, Dec. 1966, pp. 2216–2218.

[3]Spaid, F. W. and Zukoski, E. E., "A Study of the Interaction of Gasesous Jets from Transverse Slots with Supersonic External Flows," *AIAA Journal*, Vol. 6, Feb. 1968, pp. 205–212.

[4]Hsia, H. T., "Equivalence of Secondary Injection to a Blunt Body in Supersonic Flow," *AIAA Journal,* Vol. 4, Oct. 1966, pp. 1832–1834.

[5]Manela, J. and Seginer, A., "Jet Penetration Height in Transonic Flow," *AIAA Journal*, Vol. 24, Jan. 1986, pp. 67–73.

[6]Abramovich, G. N., *Theory of Turbulent Jets,* MIT Press, Cambridge, MA, 1963.

[7]Fearn, R. and Weston, R. P., "Vorticity Associated with a Jet in a Cross Flow," *AIAA Journal,* Vol. 12, Dec. 1974, pp. 1666–1671.

[8]Kamotani, Y. and Greber, I., "Experiments on a Turbulent Jet in a Cross Flow," *AIAA Journal,* Vol. 10, Nov. 1972, pp. 1425–1429.

[9]LeGrives, E., "Mixing Process Induced by the Vorticity Associated with the Penetration of a Jet into a Cross Flow," *Journal of Engineering for Power,* Vol. 100, July 1978, pp. 465–475.

[10]Karagozian, A. R., "An Analytical Model for the Vorticity Associated with a Transverse Jet," *AIAA Journal,* Vol. 24, March 1986, pp. 429–436.

[11]Karagozian, A. R., "The Flame Structure and Vorticity Generated by a Chemically Reacting Transverse Jet," *AIAA Journal,* Vol. 24, Sept. 1986, pp. 1502–1507.

[12]Karagozian, A. R., Nguyen, T. T., and Kim, C. N., "Vortex Modeling of Single and Multiple Dilution Jet Mixing in a Crossflow," *Journal of Propulsion and Power,* Vol. 2, April 1986, pp. 354–360.

[13]Karagozian, A. R. and Nguyen, T. T., "Effects of Heat Release and Flame Distortion in the Transverse Fuel Jet," *21st Symposium (Int'l.) on Combustion,* The Combustion Institute, Pittsburgh, PA, 1986, pp. 1271–1279.

[14]Moore, D. W. and Pullin, "The Compressible Vortex Pair," *Journal of Fluid Mechanics,* Vol. 195, 1987, pp. 171–204.

[15]Heister, S. D., Karagozian, A. R., and McDonough, J. M., "The Compressible Vortex Pair," *Bulletin of the American Physical Society,* Vol. 33, Nov. 1988, p. 2252.

[16]Heister, S. D., "Transverse Jets in Compressible Crossflows," Ph.D. Thesis, Univ. of California, Los Angeles, CA, 1988.

[17]Broadwell, J. E. and Briedenthal, R. E., "Structure and Mixing of a Transverse Jet Incompressible Flow," *Journal of Fluid Mechanics,* Vol. 148, 1984, pp. 405–412.

[18]Johnson, L. W. and Riess, R. D., *Numerical Analysis,* Addison Wesley, Reading, MA, 1982, p. 85.

[19]Chrans, L. J. and Collins, D. J., "Stagnation Temperature and Molecular Weight Effects in Jet Penetration," *AIAA Journal,* Vol. 8, 1970, pp. 287–293.

[20]Adamson, T. C. and Nicholls, J. A., "On the Structure of Jets from Highly Underexpanded Nozzles into Still Air," *Journal of Aerospace Sciences,* Vol. 26, Jan. 1959, pp. 16–24.

[21]Schetz, J. A. and Billig, F. S., "Penetration of Gaseous Jets Injected into a Supersonic Stream," *Journal of Spacecraft,* Vol. 3, Nov. 1966, pp. 1658–1665.